RSC Advances

PAPER

View Article Online
View Journal | View Issue

Cite this: *RSC Adv.*, 2017, **7**, 24736

Synthesis of 1,2,3-triazoles in the presence of mixed Mg/Fe oxides and their evaluation as corrosion inhibitors of API 5L X70 steel submerged in HCl†

A. Espinoza-Vázquez,[a] F. J. Rodríguez-Gómez,[a] B. I. Vergara-Arenas,[b] L. Lomas-Romero,[b] D. Angeles-Beltrán,[c] G. E. Negrón-Silva*[c] and J. A. Morales-Serna[b]

Received 31st January 2017
Accepted 1st May 2017

DOI: 10.1039/c7ra01325f

rsc.li/rsc-advances

In this work, the catalytic capacity of a Mg/Fe layered double hydroxide (LDH) and its mixed oxides to perform Huisgen cycloaddition was studied. The catalytic process was performed in the presence of sodium ascorbate, which was determinant for the success of the 1,3-cycloaddition. The obtained triazoles were evaluated as corrosion inhibitors using electrochemical impedance spectroscopy under static conditions, showing an inhibition efficiency higher than 95% at 50 ppm for some of the triazoles studied. According to the Langmuir isotherm, all the compounds synthesized and analysed exhibit a chemisorption process. Finally, the corrosion process when submerging a steel bar in 1 M HCl was studied using SEM-EDS. This experiment showed that the corrosion process decreases considerably in the presence of 50 ppm of the organic inhibitor.

1. Introduction

One of the main problems in heavy industry is the corrosion of metallic materials, which is directly reflected in economic losses for this productive sector.[1] Usually, the industrial removal of iron oxides is performed using mineral acids, of which the most used is hydrochloric acid. However, their aggressiveness accelerates the degradation of materials, causing them to dissolve in acid medium.[2]

Currently, the oil industry has resorted to organic inhibitors containing N, O and S in their basal structure to counteract the corrosion problem.[3] These types of inhibitors are obtained efficiently using easy-access synthesis pathways and are usually used at lower concentrations during the corrosion inhibition process.[4]

Among this group of organic molecules, we find triazoles, with 1,2,4-triazoles being the most used for this purpose.[5] However, special attention has been recently focused on 1,2,3-triazoles as inhibitors due to the ease with which they are synthetically obtained and their notable efficiency as inhibitors.[6] In this context, this paper reports the synthesis of 1-benzyl-4-phenyl-1,2,3-triazoles, as well as the evaluation of their capacity to inhibit corrosion in an acid aqueous medium. The study focuses on the analysis of aromatic systems substituted with electron donor groups (Fig. 1), which have not been previously studied for such applications.

Another important point to be highlighted in this study is the catalytic system used to obtain the triazoles, which are commonly synthesized in the presence of catalytic systems containing Cu(II) or Cu(I).[7] In this case, the synthesis of triazoles was performed in the presence of a Mg/Fe layered double hydroxide (LDH) (Mg/Fe hydrotalcite) and their mixed oxides. Although the Mg/Fe LDH has been used in several organic

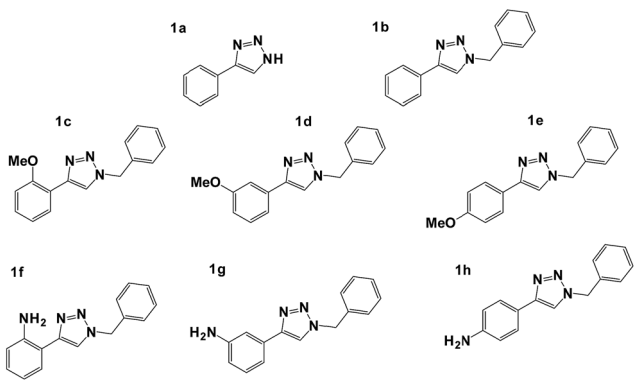

Fig. 1 Triazoles synthesised and evaluated as corrosion inhibitors.

[a]Facultad de Química, Departamento de Ingeniería Metalúrgica, Universidad Nacional Autónoma de México, Av. Universidad No. 3000, Coyoacán, C.U., Ciudad de México, C.P. 04510, Mexico

[b]Departamento de Química, Universidad Autónoma Metropolitana-Iztapalapa, Av. San Rafael Atlixco No. 186, Ciudad de México, C.P. 09340, Mexico

[c]Departamento de Ciencias Básicas, Universidad Autónoma Metropolitana-Azcapotzalco, Av. San Pablo No. 180, Ciudad de México, C.P. 02200, Mexico. E-mail: gns@correo.azc.uam.mx

† Electronic supplementary information (ESI) available. See DOI: 10.1039/c7ra01325f

transformations, it has not been studied as a catalyst in a Huisgen reaction to obtain triazoles.[7]

2. Experimental

2.1. API 5L X70 steel

API 5L X72 type steel was used, which has a metallographic preparation with the following composition nominal (wt%): C, 0.025; Mn, 1.65; Si, 0.26; Ti, 0.015; V, 0.001; Nb, 0.068; Mo, 0.175; S, 0.0025; Al, 0.045; Ni, 0.08; Cr, 0.07; Cu, 0.21 and Fe, balance.[8]

2.2. Solution preparation

A 0.01 M solution of the triazoles **1a–1h** in DMF was prepared (Fig. 1). Then, concentrations of 5, 10, 20 and 50 ppm of the inhibitor were added to the 1 M HCl corrosive solution using a Gill AC device.

2.3. Electrochemical evaluation

The potential was stabilized at 20 °C for approximately 1800 s before electrochemical impedance spectroscopy (EIS) test.

EIS: a sinusoidal potential of ±20 mV was applied in a frequency interval of 10^{-1} Hz to 10^{4} Hz, in an electrochemical cell with three electrodes. The working electrode was API 5L X70 steel, the reference electrode was saturated Ag/AgCl, and the counter electrode was graphite. The electrode surface was prepared using conventional metallography methods on an exposed area of 4.52 cm^2.

After EIS measurements, the potentiodynamic polarization curves of 5 and 50 ppm of inhibitors were obtained. The measurements covered a range of −500 mV to 500 mV regarding the open circuit potential (OCP), with a sweep velocity of 66.07 mV min^{-1} using the ACM Analysis software for data interpretation.

2.4. Characterization of surfaces by SEM-EDS

The API 5L X70 steel surface was prepared both without (blank) and with inhibitor; a 50 ppm concentration was used for a 24 h immersion time. After that experiment, the steel was washed with distilled water, dried and the surface analysed using a Zeiss SUPRA 55 VP electronic sweep microscope at 10 kV with a 300× secondary electron detector.

3. Results and discussion

3.1. Synthesis of 1,2,3-triazoles

The Mg/Fe LDH was synthesized and characterized following the steps described in the literature.[9] Then, a comparative study was performed on the use of the synthesized and calcined LDH on the multi-component reaction to obtain the 1-benzyl-4-phenyl-1,2,3-triazoles, from alkyne **2**, benzyl chloride **3** and sodium azide, in the presence or absence of sodium ascorbate with an ethanol–water mixture as solvent. The best reaction yields for each alkyne were obtained when the catalytic process was performed with calcined LDH in the presence of sodium ascorbate (Table 1). If the heterogeneous catalyst was not calcined, the yield decreased considerably (Table 1). This result is a consequence of the larger surface area of the calcined material (mixed oxides) compared with the non-calcined material (LDH).

It was also observed that the presence of sodium ascorbate was determinant for obtaining excellent yields in the cycloaddition process (Table 1). This result can be explained if we

Table 1 Synthesis of 1,2,3-triazoles in presence of LDH Mg/Fe[a]

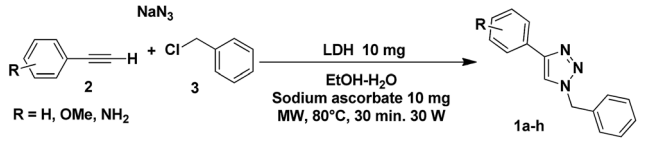

Entry	Triazole	Yield[b] (%) LDH dry	Yield[b] (%) LDH calcined
1[c]	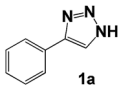 1a	40[d] 15[e]	60[d] 30[e]
2	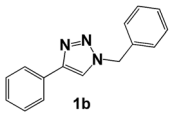 1b	48[d] 15[e]	65[d] 30[e]
3	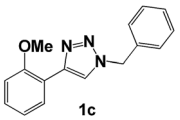 1c	40[d] 10[e]	55[d] 35[e]
4	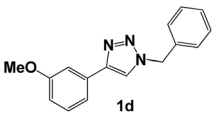 1d	40[d] 10[e]	55[d] 30[e]
5	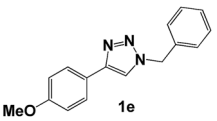 1e	45[d] 10[e]	60[d] 30[e]
6	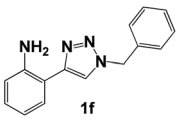 1f	30[d] 10[e]	50[d] 25[e]
7	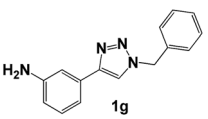 1g	25[d] 5[e]	5[d] 25[e]
8	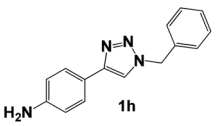 1h	25[d] 10[e]	55[d] 30[e]

[a] Reagents: alkyne **2** (1 mmol), benzyl chloride **3** (1.2 mmol), NaN_3 (1.2 mmol), catalyst (10 mg) and EtOH–H_20 (2 mL, 3 : 1). [b] Yield of isolated product after chromatographic purification. [c] The reaction was performed in the absence of benzyl chloride. [d] The reaction was performed in the presence of sodium ascorbate (10 mg). [e] The reaction was performed in the absence of sodium ascorbate.

consider that the sodium ascorbate sequesters Fe(II) from the material to reduce it to Fe(I), which is more active during the catalytic process. In this way, the global catalytic process involves a heterogeneous catalyst (LDH or Mg/Fe mixed oxides) containing Fe(II) and a homogeneous catalyst with Fe(I) associated with the ascorbate.

The above agrees with descriptions in the literature for the same organic reaction using similar catalytic systems (LDH and Cu/Al mixed oxides).[10] However, the main contribution of this work is the use of an LDH containing Fe(II) or its mixed oxides, which had never previously been used as the catalyst in a cycloaddition reaction of a terminal alkyne and a derived azide. Another important point to highlight is that the catalyst can be recovered and reused for three reaction cycles, with the same efficiency as previously described. Then, the material loses efficiency, and the yield of the organic reaction decreases considerably.

Once the triazoles **1a–1h** were synthesized, they were evaluated as corrosion inhibitors, as structurally they represent a different triazole family from the ones previously reported in the literature. In this case, the electron donor substituents are present in the aromatic ring from the alkyne (Fig. 1), in contrast to models that were previously studied in our research group, where the substituents were found in the benzylic aromatic ring.[6]

3.2. Electrochemical evaluation

The Nyquist diagram (Fig. 2) corresponds to the system without inhibitor (blank) and the different concentrations of compound **1a**. It can be observed that in the absence of the inhibitor, the semicircle formed shows a time constant reaching only a Z_{re} value of 50 Ω cm^2. Moreover, for all concentrations studied, a depressed circle is observed, denoting that the dissolution process is controlled by the charge transference resistance.[11] The deformation in the semicircles of the different concentrations is due to the material's ruggedness, the active sites or the non-homogeneity of the solids.[12] However, it shows a continuous increase in the Z_{re} value.

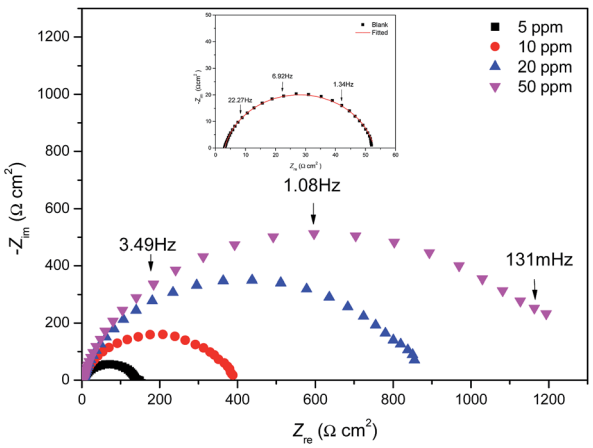

Fig. 2 Nyquist diagrams for different concentrations of **1a** on API 5L X70 submerged in 1 M HCl.

Then, using the equivalent electrical circuits, the impedance diagrams shown in Fig. 3 were adjusted to obtain the corresponding resistances and thus to calculate the inhibition efficiency. Fig. 3a is used when the system has no inhibitor, and Fig. 3b corresponds to the system when different concentrations of the inhibitor have been added.

The efficiency of the proposed inhibitors (η_{EIS}%) can be calculated using the following equation:

$$\eta_{EIS}\% = \frac{\left(\frac{1}{R_{ct}}\right)\text{blank} - \left(\frac{1}{R_{ct}}\right)\text{inhibitor}}{\left(\frac{1}{R_{ct}}\right)\text{blank}} \times 100 \qquad (1)$$

where R_{ct} blank = charge transfer resistance without inhibitor, and R_{ct} inhibitor = charge transfer resistance in presence of inhibitor.

Table 2 shows the results obtained after fitting the experimental data with the equivalent electrical circuits of Fig. 3. It can be observed that the R_{ct} increases as the inhibitor concentration increases, reaching a maximum at 50 ppm with an inhibition efficiency of 96.1%, allowing triazoles **1a** to be considered an excellent corrosion inhibitor. On the other hand, the capacitance value of the double electrochemical layer (C_{dl}) decreases due to the gradual displacement of water molecules with the compound **1a** molecules in the working electrode, which decreases the number of active sites and consequently delays the corrosion phenomenon.[13]

After demonstrating the efficiency of compound **1a**, triazole **1b**, which has a benzyl group in position 1 of the triazole ring, was studied. Fig. 4a shows the Nyquist diagram corresponding to triazole **1b** at different concentrations, with a continuous increase in the Z_{re} value reaching a maximum of ~2000 Ω cm^2 at 50 ppm. By comparing the Nyquist diagrams of inhibitors **1a** and **1b**, it can be observed that from 5 ppm, the Z_{re} value is higher for inhibitor **1b**, reaching ~500 Ω cm^2, which is attributed to the presence of the benzyl group at position 1 of the triazole ring.

Then, we examined the effect of the electron donor groups in one of the aromatic rings (Fig. 1, compounds **1c–1h**). First, we considered the three isomers (*ortho* **1c**, *meta* **1d** and *para* **1e**) containing a methoxide group (–OCH$_3$). The Nyquist diagrams for these three isomers are shown in Fig. 4.

Compound **1c** shows a continuous increase in the Z_{re} value, which is controlled by the charge transference resistance (Fig. 4b).[14]

The diameters of the semicircles are lower than for the compound without the methoxide group **1b**, which is attributed to the presence of oxygen with pairs of free, unshared electrons.

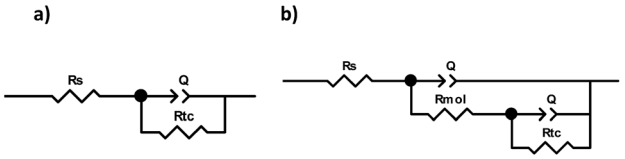

Fig. 3 Equivalent electrical circuits used in the system with and without inhibitor.

Table 2 Electrochemical parameters for **1a** as corrosion inhibitor at 20 °C on API 5L X70 submerged in 1 M HCl

C/ppm	0	5	10	20	50
R_s/Ω cm^2	5.0	5.3	5.1	5.1	5.1
±SD	0.00	0.02	0.01	0.01	0.01
n	0.8	0.9	0.8	0.9	0.9
C_{dl}/μF cm^{-2}	1490.0	147.9	147.2	147.1	143.6
±SD	0.0	23.3	53.4	64.2	39.3
R_{ct}/Ω cm^2	50.0	167.3	437.3	919.9	1285.3
±SD	0.0	23.3	53.4	64.2	39.3
η_{EIS}/%	—	69.5	88.4	94.5	96.1
±SD	—	4.4	1.4	0.4	0.1

These pairs of electrons can be located in a p orbital parallel to the p orbitals forming the aromatic system, which allows the generation of resonant structures with high electronic density in the aromatic ring.

The Nyquist diagram for triazoles **1d** and **1e** (Fig. 4c and d) shows the sweep of the different concentrations analysed. In both cases, two time constants can be observed, one attributed to the charge transference resistance and the other to the inhibitor's molecules.[15] Likewise, it can be observed that the Z_{re} value does not show large variation. Based on these results, it can be inferred that the presence of a methoxide group in the *ortho*, *meta* and *para* positions of the aromatic ring is not involved in the increase of the inhibition capacity, based on comparison to triazole **1b**.

Table 3 shows the different results obtained after fitting to the experimental data, revealing that the corrosion inhibition increases when the inhibitor concentration increases. In contrast, the presence of a methoxide group in the chemical structure decreases the charge transfer resistance value, and therefore, the corrosion inhibition decreases.

Next, the 1,2,3-triazoles where the methoxide group (–OMe) was substituted with an amine (–NH_2) were evaluated. The Nyquist diagrams for triazoles **1f**, **1g** and **1h** are shown in Fig. 5. All these diagrams show an increase in the Z_{re} value as the inhibitor concentration increases. Based on these diagrams, it can be deduced that the amine group (–NH_2) in the *ortho* position favourably influences the corrosion process (Fig. 5).

Again, after the experimental data fitting, Table 4 shows the electrochemical parameters for triazoles **1f**, **1g** and **1h**. The R_{ct} values increase as the inhibitor concentration increases, in contrast to what happens to the C_{dl} values, which decrease. This result is attributed to the displacement of water molecules by the inhibitor molecules.[16] On the other hand, the second time constant proposed in the Nyquist diagrams is attributed to the resistance of organic molecules (R_{mol}) for compounds **1f** and **1g**.

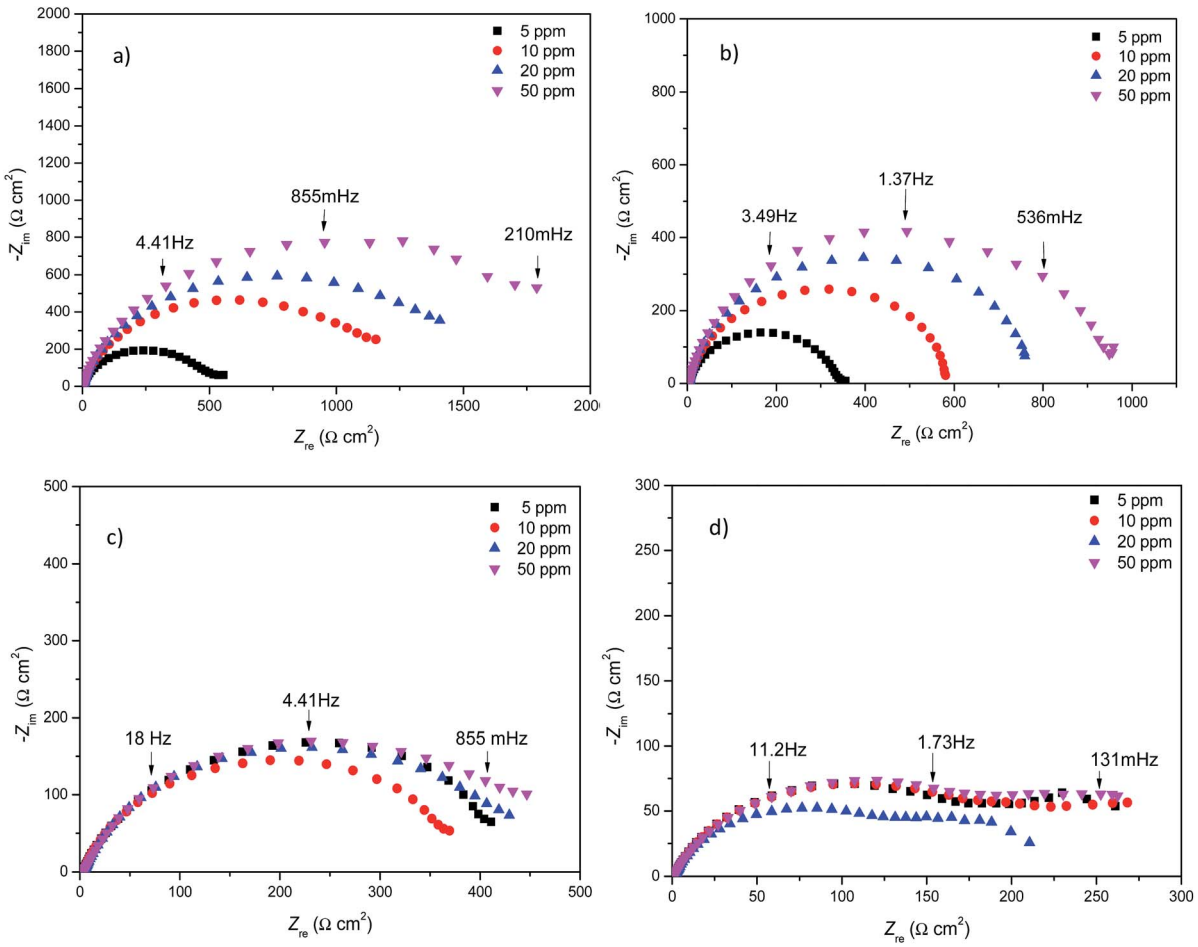

Fig. 4 Nyquist diagrams for different concentrations of (a) **1b**, (b) **1c**, (c) **1d** and (d) **1e** on API 5L X70 submerged in 1 M HCl.

Table 3 Electrochemical parameters for **1b–1e** as corrosion inhibitors at 20 °C on API 5L X70 submerged in 1 M HCl[a]

Triazole	C/ppm	R_s/Ω cm^2	±SD	n	C_{dl}/μF cm^{-2}	±SD	R_{ct}/Ω cm^2	±SD	η_{EIS}/%	±SD
1b	0	5	0	0.8	1490	0	50	0		
	5	4.3	0.0	0.9	112.4	5.9	683.7	126.9	92.4	1.5
	10	4.1	0.0	0.9	107.8	1.8	1350.0	66.4	96.3	0.2
	20	4.1	0.0	0.9	110.0	3.8	1693.0	101.4	97.0	0.2
	50	4.2	0.0	0.9	116.9	1.9	2306.0	174.4	97.8	0.2
1c	5	4.2	0.0	0.8	119.7	9.9	416.7	56.9	87.8	1.7
	10	4.2	0.0	0.9	125.8	4.3	638.9	42.6	92.1	0.5
	20	4.2	0.0	0.8	127.4	3.3	820.6	29.8	93.9	0.2
	50	4.2	0.0	0.8	129.6	4.5	1046.8	68.4	95.2	0.3
1d	5	1.6	0.4	0.8	106.6	13.3	420.5	33.8	88.0	0.9
	10	1.7	0.3	0.7	103.3	21.1	421.1	26.0	88.1	0.8
	20	2.4	0.5	0.7	112.9	12.9	471.5	14.0	89.4	0.3
	50	3.0	0.3	0.7	117.0	11.9	498.5	5.9	90.0	0.1
1e	5	0.6	0.0	0.6	273.4	34.5	131.2	14.0	73.3	2.2
	10	0.7	0.2	0.9	309.1	157.7	240.4	19.6	79.1	1.8
	20	0.8	0.1	0.9	391.4	157.8	248.7	77.2	78.0	6.3
	50	0.9	0.1	0.9	369.5	88.0	237.0	13.9	78.8	1.2

[a] SD = standard deviation of at least three measurements.

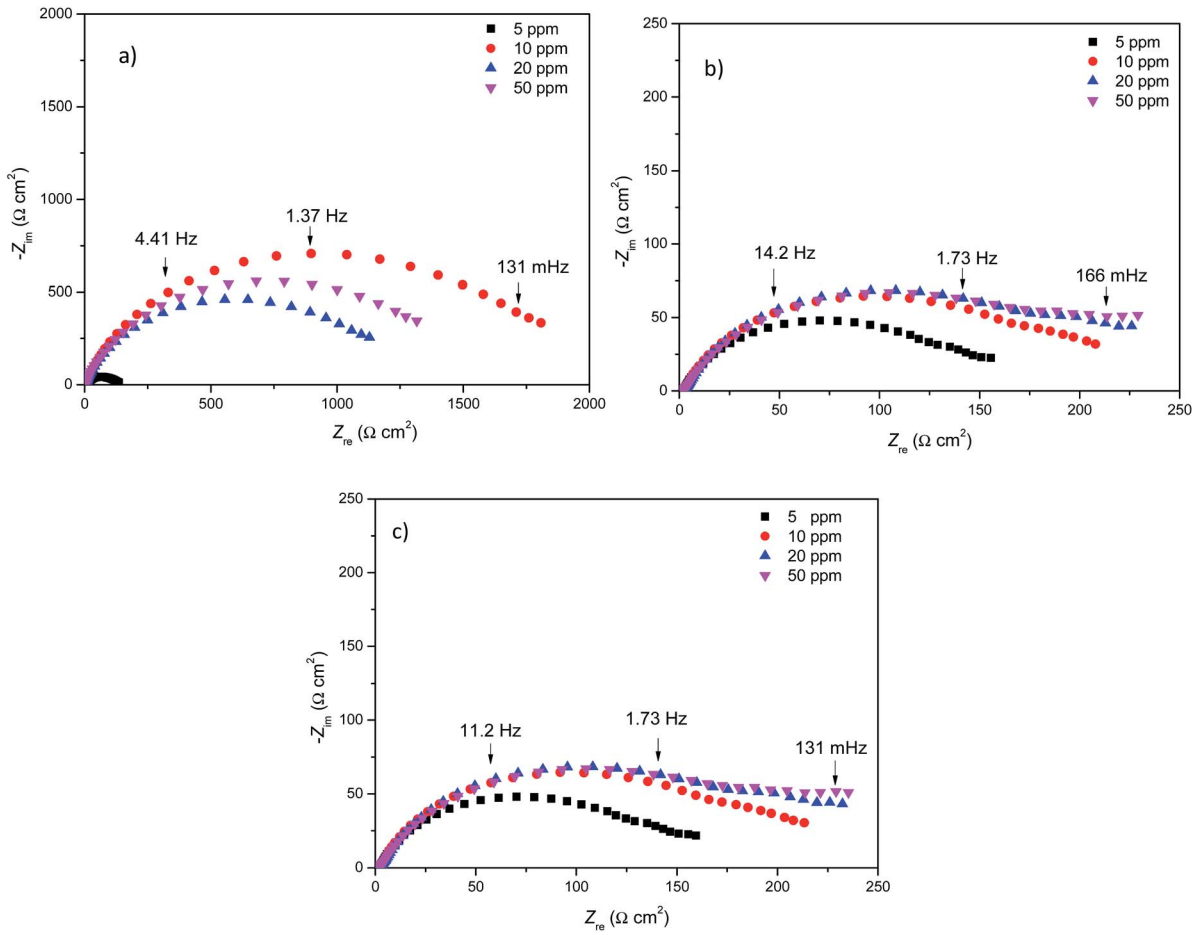

Fig. 5 Nyquist diagrams for different concentrations of (a) **1f**, (b) **1g** and (c) **1h** on API 5L X70 submerged in 1 M HCl.

Fig. 6 shows the comparison of the different 1,2,3-triazoles. The presence of the benzyl group at position 1 of the triazole ring is determinant for obtaining excellent inhibition results with compound **1b** ($\eta \sim 96.8\%$ at 50 ppm, Fig. 6a). The presence of methoxide or amine electron donor groups at the *meta* or *para* position in one of the aromatic rings does not have a notable

Table 4 Electrochemical parameters at different concentrations for **1f–1h** as corrosion inhibitors at 20 °C on API 5L X70 in 1 M HCl

Triazole	C/ppm	R_s/Ω cm^2	±SD	n	C_{dl}/μF cm^{-2}	±SD	R_{ct}/Ω cm^2	±SD	R_{mol}/Ω cm^2	±SD	η_{EIS}/%	±SD
1f	0	5.0	0.0	0.8	1490.0	0.0	50.0	0.0	0.0	—		
	5	10.7	0.1	0.9	66.7	19.1	419.4	210.4	117.7	91.3	80.5	5.2
	10	10.7	0.2	0.9	72.3	17.6	1937.0	131.1	170.1	85.1	97.4	0.2
	20	5.3	0.1	0.9	138.8	26.8	1076.2	100.5	205.9	10.2	95.3	0.4
	50	5.3	0.1	0.9	143.4	72.3	1545.0	28.3	115.9	8.6	96.8	0.1
1g	5	7.3	0.0	0.9	187.2	45.2	336.9	93.1	26.0	13.2	83.6	5.5
	10	7.4	0.0	0.9	170.0	12.6	376.7	88.6	95.6	76.2	85.9	3.4
	20	6.7	0.5	0.9	163.3	5.2	473.7	23.0	1.0	0.2	89.4	0.5
	50	7.0	0.0	0.9	167.1	1.7	460.2	36.9	3.2	3.0	89.1	0.8
1h	5	1.6	0.0	0.7	336.7	11.7	164.5	3.6	—	—	69.6	0.7
	10	1.7	0.1	0.7	283.2	16.3	220.8	11.0	—	—	77.3	1.1
	20	1.8	0.0	0.7	296.5	18.7	238.8	11.8	—	—	79.0	1.0
	50	1.7	0.1	0.7	331.2	17.1	237.9	1.9	—	—	79.0	0.2

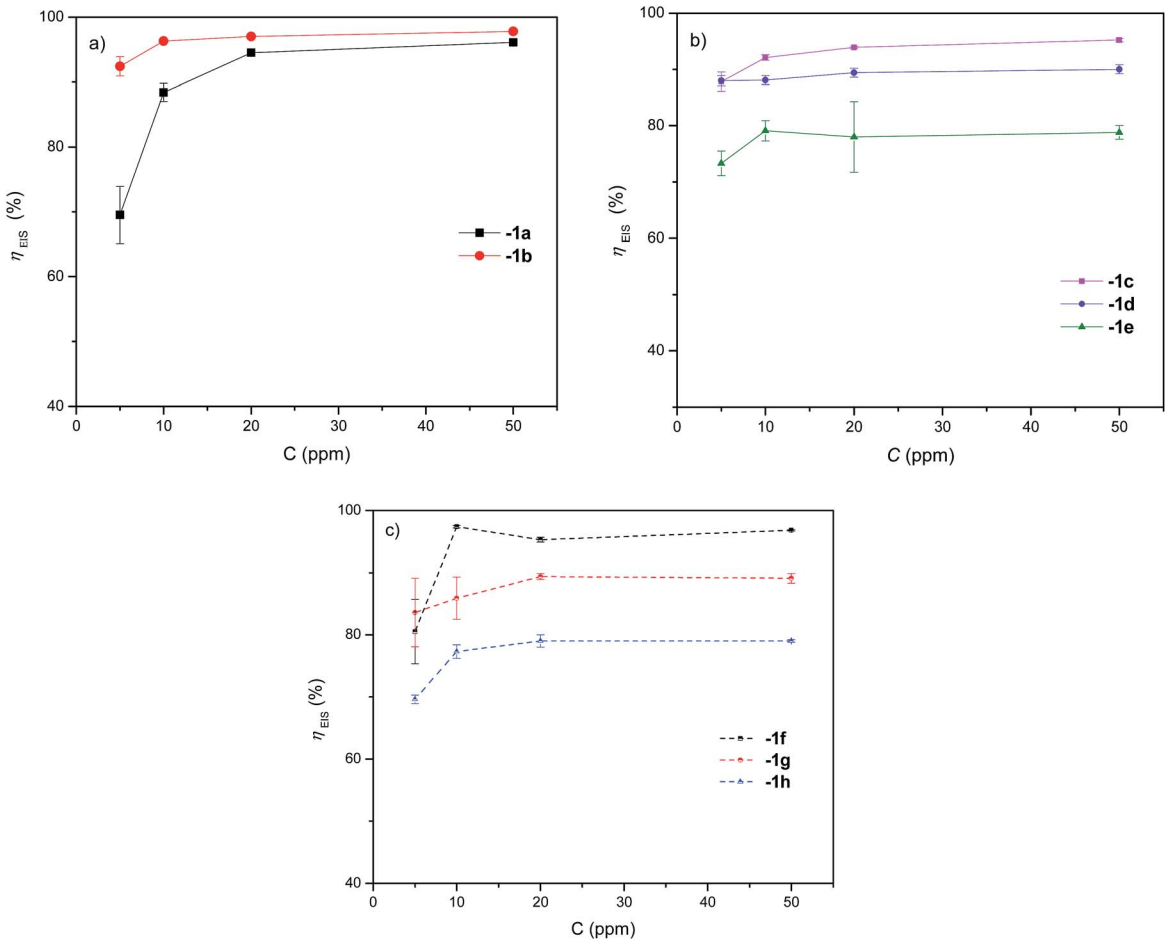

Fig. 6 Variation of the inhibition efficiency by EIS technique of **1a**, **1b** and derivatives **1c–1h** as a function of API 5L X70 steel concentration submerged in 1 M HCl.

impact on the efficiency of the system when inhibiting corrosion (Fig. 6b and c). However, electron donor groups at the *ortho* position to influence the corrosion inhibition process; the best inhibitors are **1c** with $\eta \sim 93.6\%$ and **1f** with $\eta \sim 96.8\%$ at 50 ppm.

3.3. Polarization curves

Tafel polarization curves of API 5L X70 steel at 5 and 50 ppm of triazoles are shown in Fig. 7. The corrosion potential (E_{corr}), corrosion current density (i_{corr}), Tafel anodic slopes (β_a), Tafel cathodic slopes (β_c), and inhibition efficiency (η), are shown in Table 5.

The inhibition efficiency of the organic compounds (triazoles) were calculated by:

$$\eta_{pol} = \left(1 - \frac{i_{corr\ inhibitor}}{i_{corr\ uninhibitor}}\right) \times 100 \quad (2)$$

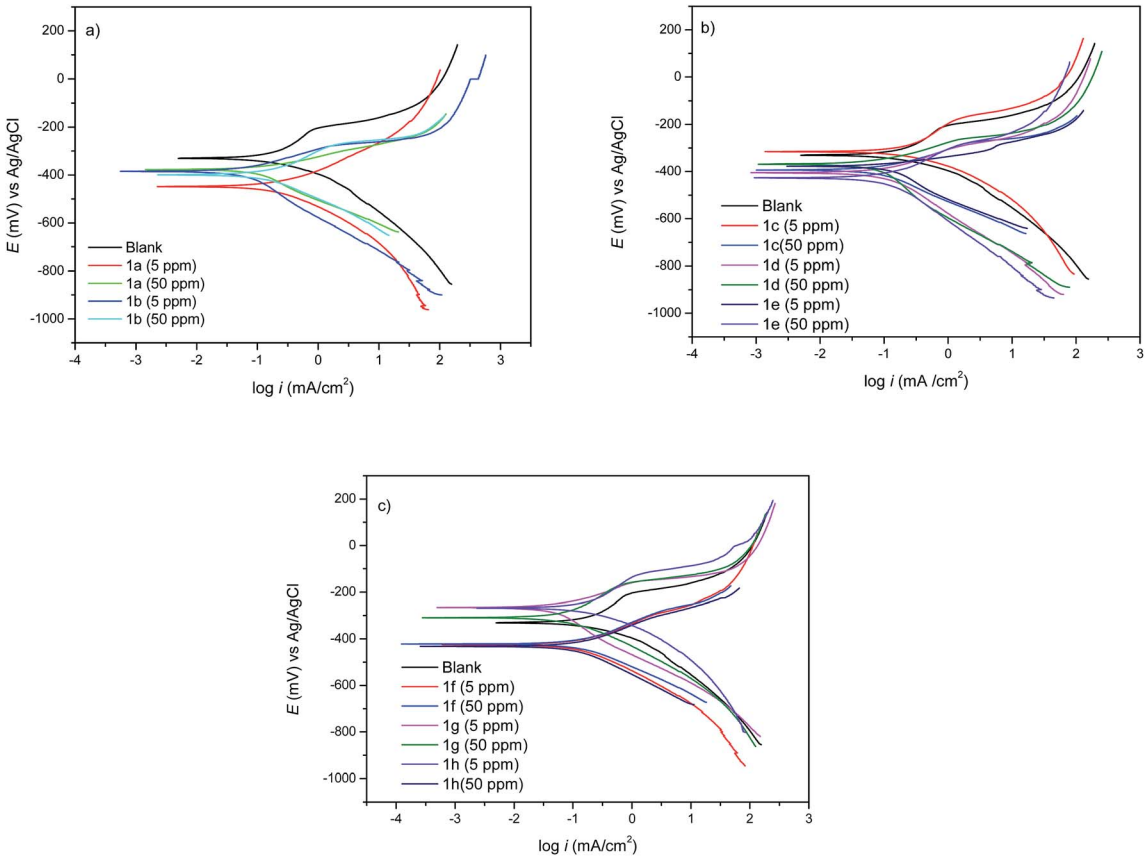

Fig. 7 Potentiodynamic polarization curves at different 1,2,3-triazoles derivatives concentrations for API 5L X70 steel submerged in 1 M HCl.

Table 5 Electrochemical parameters by the potentiodynamic polarization technique for API 5L X70 steel submerged in 1 M HCl in the presence of 1,2,3-triazoles derivatives

Inhibitor	C/ppm	E_{corr}/mV *vs.* Ag/AgCl	β_a/mV dec^{-1}	β_c/mV dec^{-1}	i_{corr}/mA cm^{-2}	η_{pol}/%
BLANK	—	−330.97	173.4	125.1	0.5303	—
1a	5	−428.7	84.5	132.9	0.1320	75.1
	50	−377.5	99.0	36.4	0.0518	90.2
1b	5	−385.7	156.0	52.1	0.0561	89.4
	50	−373.7	111.0	59.2	0.0602	88.7
1c	5	−385.0	155.0	63.8	0.0841	84.1
	50	−393.9	111.0	76.8	0.0640	87.9
1d	5	−405.4	184.1	79.9	0.1159	78.1
	50	−371.2	215.1	65.5	0.0743	86.0
1e	5	−377.7	118.6	35.9	0.0688	87.0
	50	−425.0	195.8	129.2	0.1160	78.1
1f	5	−421.0	113.0	88.0	0.1354	74.5
	50	−264.5	142.4	50.9	0.0338	93.6
1g	5	−265.4	141.5	67.5	0.0336	93.7
	50	−309.3	127.7	88.1	0.1050	80.2
1h	5	−432.1	127.6	95.0	0.1127	78.7
	50	−472.0	113.5	137.1	0.1035	80.5

where $i_{corr\ inhibitor}$ is the corrosion current density with inhibitor and $i_{corr\ uninhibited}$ is the corrosion current density in the absence of inhibitor.

In Fig. 7a–c for triazoles derivatives under static conditions, it can be observed how the current density decreases in their presence, which suggests that it is retarding the corrosion process due to the protective film formed by the inhibitor on the metallic surface.[17]

The results shown in Table 5 correspond to the corrosion potential (E_{corr}) in the presence of the inhibitor **1b**, **1c**, **1d** and

1g. The difference between the values of blank and the inhibitors is less than 85 mV, which suggests[18] that triazoles show a mixed predominantly anodic type inhibition. On the other hand, inhibitors **1f** and **1h** show a cathodic type behaviour.

3.4. Adsorption process

After calculating the electrochemical parameters for the different organic compounds under static conditions, it is necessary to describe the interaction of the inhibitor with the metallic surface, calculating the surface coverage (θ) using the eqn (3) employing the inhibition efficiency (η) from eqn (1).[19]

$$\theta = \frac{\eta_{EIS}}{100} \quad (3)$$

where: η_{EIS} is inhibition efficiency by EIS technique.

In the literature, there are several adsorption models relating the coating degree to the metallic surface; including the Temkin, Freundlich, Frumkin[20] or Langmuir models.[21] The latter was used in this study. Once the fitting was performed with the Langmuir adsorption model (eqn (4)), it was observed that it possesses a linear fit, given that it obtained a correlation coefficient (R^2) close to 1.

$$\frac{C}{\theta} = \frac{1}{k_{ads}} + C \quad (4)$$

where C = concentration and k_{ads} = adsorption constant.

Fig. 8a–c show the Langmuir isotherm model for each of the corrosion inhibitors, showing that the ΔG°_{ads} value of organic compounds **1b–1e** is higher than -40 kJ mol^{-1} (Table 6). These values, according to the literature reports,[22] represent a chemisorption interaction of the inhibitor with the metallic surface. It is noteworthy that the inhibitor **1a** exhibits a ΔG°_{ads} between -20 kJ mol^{-1} and -40 kJ mol^{-1}, which indicates the simultaneous physical and chemical adsorption of this molecule on mild steel surface immersed in HCl.

Table 6 Adsorption parameters of derivatives of 1,2,3-triazoles submerged in 1 M HCl

Inhibitors	ln k_{ads}	ΔG°_{ads} kJ mol^{-1}
1a	15.88	−38.71
1b	17.83	−43.46
1c	17.13	−41.77
1d	18.05	−44.00
1f	17.13	−41.77
1g	17.83	−43.46
1h	17.04	−41.53
1e	17.83	−43.46

3.5. SEM-EDS

Fig. 9 shows the microscopy pictures and the corresponding chemical analysis for the polished metal, in the presence and absence of the inhibitor, to confirm the efficiency of each compound obtained by the EIS. The polished steel consists of Fe, Mn, C and Si (Fig. 9a). When the metal was submerged in hydrochloric acid, it was observed that in addition to the steel composition, O and Cl are present as a consequence of the

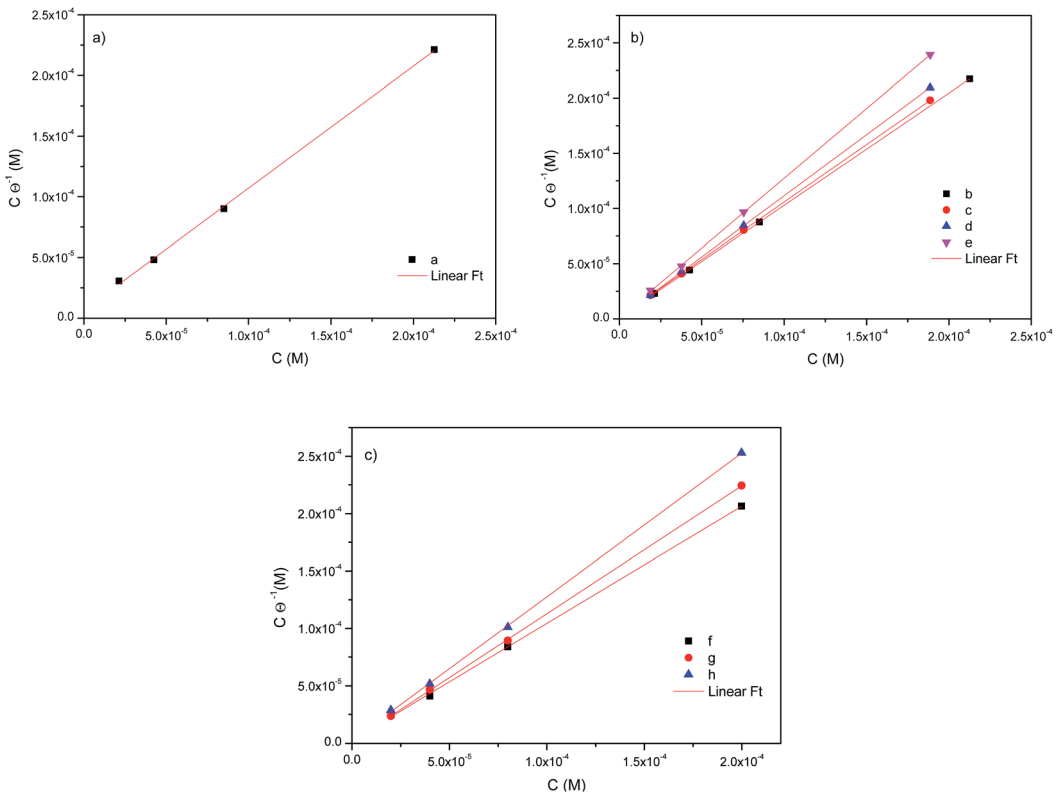

Fig. 8 Langmuir isotherm of triazoles **1a–1h** as corrosion inhibitors of the surface of API 5L X70 submerged in 1 M HCl.

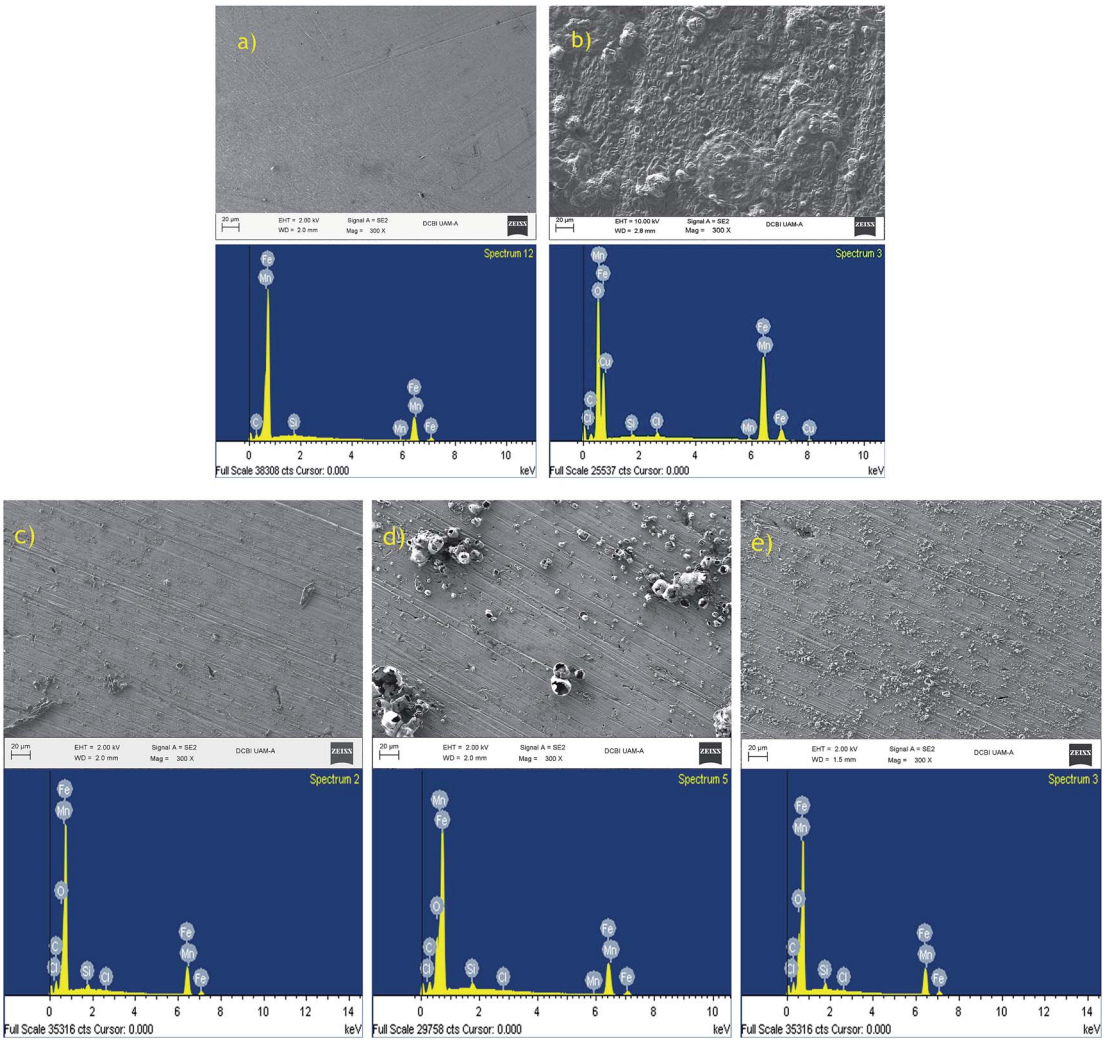

Fig. 9 SEM-EDX spectra of API 5L X70 steel: (a) polished steel, (b) in presence of corroding medium, and in presence of 50 ppm (c) **1b**, (d) **1c** and (e) **1f**.

corrosion phenomenon (Fig. 9b). In the microscopy pictures corresponding to samples with the inhibitor (Fig. 9c–e), a decrease in corrosion can be observed.

To determine the elements present in API 5L X70 steel surface after 5 hours of exposure to 1 M HCl, EDX analysis were used. Before the corrosion test, the peaks are related to the elements present in the API 5L X70 steel (Table 7). In the absence of inhibitors, the spectra exhibit the peaks of oxygen and chloride which regarding to polished API 5L X70 do not have. The spectra of API 5L X70 steel immersed in 1 M HCl containing 50 ppm of **1b**, **1c** and **1f** inhibitors show that the amount of oxygen and chloride decreases, probably due to the formation of a triazole derivative film on the surface of steel.

3.6. Inhibition mechanism

In the inhibition mechanism two main types of interaction exist that can describe the adsorption of the inhibitors: physisorption and chemisorption. Several authors describe the inhibition mechanism by protonated species in acid medium (Scheme 1a), which are attracted toward the solid/liquid interface to form a protective film, preventing the metal from interacting with the aggressive medium (physisorption).[23] On the other hand, the adsorption of 1,2,3-triazoles can also occur due to the interactions between the d-orbital of iron atoms (coordinate type bond), with the lone sp^2 electron pairs present on the heteroatoms of the inhibitor (chemisorption, Scheme

Table 7 Content of elements obtained from EDX spectra

	% atomic				
Element	Steel	Steel + HCl	**1b**	**1c**	**1f**
C	14.21	9.51	15.84	11.49	12.57
O	—	51.62	7.09	16.11	19.31
Si	0.45	0.3	1.23	1.19	1.2
Cl	—	0.67	0.1	—	0.24
Mn	0.82	0.31	—	—	—
Fe	84.5	37.59	92.53	71.21	66.67

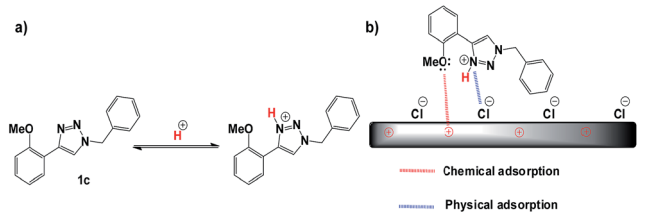

Scheme 1 (a) Protonation and (b) schematic adsorption model of the triazole **1c** on API 5L X70 surface in 1 M HCl.

1b). In this case, both models can help to explain the behaviour of triazoles as corrosion inhibitors.

4. Conclusions

The synthesis of 1,2,3-triazoles is usually performed in the presence of Cu(I) and Cu(II) salts. However, in this study, we demonstrated that a solid catalytic material such as a Mg(II)/Fe(III) hydrotalcite and its mixed oxides can catalyse the Huisgen cycloaddition with good yields. After the catalytic process, it is possible to recover the heterogeneous catalyst for reuse in two additional reaction cycles with the same efficiency.

On the other hand, the 1-benzyl-4-phenyl-1,2,3-triazoles obtained were evaluated as corrosion inhibitors, demonstrating that the presence of activator groups in the *ortho* position of one of the aromatic rings in the inhibitor system influences the corrosion inhibition process of API 5L X70 steel submerged in 1 M HCl. The adsorption of the studied compounds, using the Langmuir equation, reveals that the inhibitor molecule blocks the active sites by a chemisorption process.

Acknowledgements

The authors would like to thank Consejo Nacional de Ciencia y Tecnología (CONACyT project-239938) for financial support. AEV is grateful to DGAPA-UNAM for the Postdoctoral Grant. FJRG is grateful to FQ-UNAM for the PAIP support. JAMS acknowledges support by the Royal Society (UK), Newton Fellowship Alumni program.

Notes and references

1 D. A. Winkier, M. Breedon, P. White, A. E. Hughes, E. D. Sapper and I. Cole, *Corros. Sci.*, 2016, **106**, 229.

2 (*a*) K. Wan, P. Feng, B. Hou and Y. Li, *RSC Adv.*, 2016, **6**, 77515; (*b*) S. M. Shaban, *RSC Adv.*, 2016, **6**, 39784.

3 (*a*) E. Garcia-Ochoa, S. J. Guzmán-Jiméz, J. G. Hernández, T. Pandiyan, J. M. Vásquez-Pérez and J. Cruz-Borbolla, *J. Mol. Struct.*, 2016, **1119**, 314; (*b*) M. A. Hegazy, S. S. Abd El Rehim, A. M. Badawi and M. Y. Ahmed, *RSC Adv.*, 2015, **5**, 49070; (*c*) M. A. Hegazy, *J. Mol. Liq.*, 2015, **208**, 227; (*d*) H. Tian, Y. Frank Cheng, W. Li and B. Hou, *Corros. Sci.*, 2015, **100**, 341; (*e*) M. S. Shihab and A. F. Mahmood, *Russ. J. Appl. Chem.*, 2016, **89**, 505; (*f*) A. L. Chong, J. I. Mardel, D. R. MacFarlane, M. Forsyth and A. E. Somers, *ACS Sustainable Chem. Eng.*, 2016, **4**, 1746; (*g*) M. H. Keshavarz, K. Esmaelpour, A. N. Golikand and Z. Shirazi, *Z. Anorg. Allg. Chem.*, 2016, **642**, 906.

4 (*a*) S. K. Saha, A. Dutta, P. Ghosh, D. Sukul and P. Banerjee, *Phys. Chem. Chem. Phys.*, 2016, **18**, 17898; (*b*) M. Shabani, N. M. Behpour, F. Sadat, R. M. Hamadanianb and V. Nejadshafiee, *RSC Adv.*, 2015, **5**, 23357.

5 (*a*) M. El Bakri, R. Touir, N. Dkhireche, M. Ehn Touhami, A. Rochdi and A. Zarrouk, *Arabian J. Sci. Eng.*, 2016, **41**, 75; (*b*) D. K. Ivanou, K. A. Yasakau, S. Kallip, A. D. Lisenkov, M. Starkevich, S. V. Lamaka, M. G. S. Ferreira and M. L. Zheludkevich, *RSC Adv.*, 2016, **6**, 12553; (*c*) G. Rajkunar and M. G. Sethuraman, *Res. Chem. Intermed.*, 2016, **42**, 1809; (*d*) J. Balaji and M. G. Sethuraman, *Res. Chem. Intermed.*, 2016, **42**, 1328.

6 (*a*) A. Espinoza-Vázquez, F. J. Rodriguez-Gómez, R. González-Olvera, D. Angeles-Beltran, D. Mendoza-Espinosa and G. E. Negrón-Silva, *RSC Adv.*, 2016, **18**, 72885; (*b*) A. Espinoza-Vázquez, G. E. Negrón-Silva, R. González-Olvera, D. Angeles-Beltran, M. Romero-Romo and M. Palomar-Pardavé, *Arabian J. Sci. Eng.*, 2017, **42**, 163; (*c*) A. Espinoza-Vázquez, G. E. Negrón-Silva, R. González-Olvera, D. Angeles-Beltran, H. Herrera-Hernández, M. A. Romero-Romo and M. E. Palomar-Pardavé, *Mater. Chem. Phys.*, 2014, **145**, 407.

7 For recent reviews about synthesis of 1,2,3-triazole, see:(*a*) H. B. Jalani, A. Ç. Karagöz and S. B. Tsogoeva, *Synthesis*, 2017, **49**, 29; (*b*) C. Wang, D. Ikhlef, S. Kahlal and J.-Y. Saillard, *Coord. Chem. Rev.*, 2016, **316**, 1; (*c*) S. Chassaing, V. Bénéteau and P. Pale, *Catal. Sci. Technol.*, 2016, **6**, 923; (*d*) V. Castro, H. Rodríguez and F. Albericio, *ACS Comb. Sci.*, 2016, **18**, 1; (*e*) Z.-J. Zheng, D. Wang, Z. Xu and L.-W. Xu, *Beilstein J. Org. Chem.*, 2015, **11**, 2557; (*f*) A. Laurina, R. Delisi, F. Mingoia, A. Terenzi, A. Martorana, G. Barone and M. Almerico, *Eur. J. Org. Chem.*, 2014, 3289.

8 M. A. Mohtadi-Bonab, J. A. Szpunar, R. Basu and M. Eskandari, *Int. J. Hydrogen Energy*, 2015, **40**, 1096.

9 (*a*) K. Morimoto, K. Tamura, H. Yamada, T. Sato and M. Suzuki, *Appl. Clay Sci.*, 2016, **121–122**, 71; (*b*) A. Dias, L. Cunha and A. C. Vieira, *Mater. Res. Bull.*, 2011, **46**, 1346; (*c*) N. B.-H. Abdelkader, A. Bentouami, Z. Derriche, N. Bettahar and L.-C. de Ménorval, *Chem. Eng. J.*, 2011, **169**, 231; (*d*) W. Meng, F. Li, D. G. Evans and X. Duan, *Mater. Res. Bull.*, 2004, **39**, 1185; (*e*) J. Das, D. Das, G. P. Dash and K. M. Parida, *J. Colloid Interface Sci.*, 2002, **251**, 26.

10 R. González-Olvera, C. I. Urquiza-Castro, G. E. Negrón-Silva, D. Ángeles-Beltrán, L. Lomas-Romero, A. Gutiérrez-Carrillo, V. H. Lara, R. Santillán and J. A. Morales-Serna, *RSC Adv.*, 2016, **6**, 63660.

11 (*a*) K. Kermannezhad, A. C. Najafi, M. M. Mohsen and B. Rezae, *Chem. Eng. J.*, 2016, **306**, 849; (*b*) P. Singh, V. Srivastava and M. A. Quraishi, *J. Mol. Liq.*, 2016, **216**, 164; (*c*) K. H. Hassan, A. A. Khadom and N. H. Kurshed, *S. Afr. J. Chem. Eng.*, 2016, **22**, 1.

12 A. Khadiri, R. Saddik, K. Bekkouche, A. Aouniti, B. Hammouti, N. Benchat, M. Bouachrine and R. Solmaz, *J. Taiwan Inst. Chem. Eng.*, 2016, **58**, 552.

13 (*a*) C. Verma, M. A. Quraishi and A. Singh, *Journal of Taibah University for Science*, 2016, **10**, 718; (*b*) F. Xu, J. Duan, S. Zhang and B. Hou, *Mater. Lett.*, 2008, **62**, 4072.

14 (*a*) F. Bentiss, C. Jama, B. Mernari, H. E. Attari, L. E. Kadi, M. Lebrini, M. Traisnel and M. Lagrenée, *Corros. Sci.*, 2009, **51**, 1628; (*b*) H.-L. Wang, R.-B. Liu and J. Xin, *Corros. Sci.*, 2004, **46**, 2455.

15 (*a*) A. Döner, R. Solmaz, M. Özcan and G. Kardaş, *Corros. Sci.*, 2011, **53**, 2902; (*b*) M. A. Hegazy, M. Abdallah, M. K. Awad and M. Rezk, *Corros. Sci.*, 2014, **81**, 54; (*c*) S. John and A. Joseph, *Mater. Chem. Phys.*, 2012, **133**, 1083.

16 (*a*) A. Y. Musa, A. A. H. Kadhum, A. M. Bakar and M. T. Sobri, *Corros. Sci.*, 2010, **52**, 3331; (*b*) D. M. Gurudatt, K. N. Mohana and H. C. Tandon, *Materials Discovery*, 2015, **2**, 24.

17 N. Kumar, C. Verma, M. A. Quraishi and A. K. Mulherjee, *J. Mol. Liq.*, 2016, **215**, 47.

18 S. Shaban, A. Abd-Elaal and S. Tawfik, *J. Mol. Liq.*, 2016, **216**, 392.

19 (*a*) Z. Tao, W. He, S. Wang, S. Zhang and G. Zhou, *Corros. Sci.*, 2012, **60**, 205; (*b*) Z. Hu, Y. Meng, X. Ma, H. Zhu, J. Li, C. Li and D. Cao, *Corros. Sci.*, 2016, **112**, 563.

20 (*a*) C. Verma, M. A. Quraishi and A. Singh, *J. Mol. Liq.*, 2015, **212**, 804; (*b*) P. Singh, M. J. Makowska, P. Slovensky and M. A. Quraishi, *J. Mol. Liq.*, 2016, **220**, 71; (*c*) M. S. Salih and A.-D. H. Hussien, *J. Mol. Struct.*, 2014, **1076**, 658; (*d*) T. C. Krishnamurthy, K. N. M. Shetty and H. T. Chander, *J. Mol. Liq.*, 2015, **211**, 1026.

21 (*a*) M. Yadav, S. Kumar, R. R. Sinha, I. Bahadur and E. E. Ebenso, *J. Mol. Liq.*, 2015, **211**, 135; (*b*) A. Yurt, B. Duran and H. Dal, *Arabian J. Chem.*, 2014, **7**, 732.

22 (*a*) N. Yilmaz, A. Fitoz, Ü. Ergun and K. C. Emregül, *Corros. Sci.*, 2016, **111**, 110; (*b*) M. I. Awad, *J. Appl. Electrochem.*, 2006, **36**, 1163; (*c*) H. Jafari, *Trans. Indian Inst. Met.*, 2016, **69**, 805; (*d*) A. Teimouri, N. Soltani and A. N. Chermahini, *Front. Chem. Sci. Eng.*, 2011, **5**, 43.

23 (*a*) G. Karthik, M. Sundaravadivelu and P. Rajkumar, *Res. Chem. Intermed.*, 2015, **41**, 1543; (*b*) M. Farsak, H. Keles and M. Keles, *Corros. Sci.*, 2015, **98**, 223.

